Journal of Physics: Conference Series

PAPER • **OPEN ACCESS**

Modeling the transient aerodynamic effects during the motion of a flexible trailing edge

To cite this article: T Wolff and J R Seume 2016 *J. Phys.: Conf. Ser.* **753** 082038

Modeling the transient aerodynamic effects during the motion of a flexible trailing edge

T Wolff and J R Seume

ForWind - Center for Wind Energy Research, Leibniz Universitaet Hannover,
Institute of Turbomachinery and Fluid Dynamics - TFD,
Appelstr. 9, 30167 Hanover, Germany

E-mail: wolff@tfd.uni-hannover.de

Abstract. Wind turbine blades have been becoming longer and more slender during the last few decades. The longer lever arm results in higher stresses at the blade root. Hence, the unsteady loads induced by turbulence, gust, or wind shear increase. One promising way to control these loads is to use flexible trailing edges near the blade tip. The unsteady effects which appear during the motion of a flexible trailing edge must be considered for the load calculation during the design process because of their high influence on aeroelastic effects and hence on the fatigue loads. This is not yet possible in most of the wind turbine simulation environments. Consequently, an empirical model is developed in the present study which accounts for unsteady effects during the motion of the trailing edge. The model is based on Fourier analyses of results generated with Reynolds-Averaged Navier-Stokes (RANS) simulations of a typical thin airfoil with a deformable trailing edge. The validation showed that the model fits Computational Fluid Dynamics (CFD) results simulated with a random time series of the deflection angle.

1. Introduction

During the last few decades, the length of wind turbine rotor blades has increased in response to demand for higher power generation per wind turbine [1]. Complex flow environments with wind shear, turbulence, and gusty wind conditions cause high unsteady loading on increasingly long and slender rotor blades [2]. Due to the longer lever arm which accompanies the longer blades, higher stress variations arise, particularly at the blade root. One way to reduce stress variations on the blade root is to reduce the dynamic forces acting near the blade tip region, which is achieved by keeping the lift coefficient in this region constant. Airfoils with morphing trailing edges applied to the outer blade region of the wind turbine are a promising method to actively control the lift coefficient and consequently the loads acting on the blade [3].

The main control objective for deformable trailing edges on wind turbines is to reduce the fatigue loads acting on the wind turbine, in order to adjust the lift in response to transient flow conditions [4]. Studies of trailing-edge flaps and deformable trailing edges applied to wind turbine blades have already been carried out, including numerical and experimental investigations. The wind tunnel tests carried out by Pechlivanoglou et al. [5] and also by Bak et al. [6] showed that the lift of a wind turbine airfoil can be directly controlled by adaptive trailing-edge geometry.

Troldborg [7] carried out extensive simulations using the 2D incompressible RANS solver EllipSys2D, in order to derive an optimal trailing-edge geometry. In addition to the parameter study based on steady-state simulations, transient flow phenomena were investigated by

simulating harmonic pitch oscillations and/or oscillatory motions of the deformable trailing edge. In conclusion, Troldborg's work suggests that a curved trailing edge with a relative length between 5% and 10% of the chord length is a good compromise between the ability to control the lift, and the actuator power needed to deflect the trailing edge. By contrast, the optimal relative length of the deflected trailing edge was found to be of 20% by Wolff et al. [8], who performed two-dimensional RANS simulations using the solver FLOWer. The different optima are a result of different objectives: Troldborg chose a configuration with low drag and flap hinge moment, which met the requirements to control a changing lift coming from a given wind field. Wolff et al. found an optimum value at which the ratio between the force needed to deflect the trailing edge and the gained lift has a minimum.

Wolff and Seume [9] showed that the dynamic values of the aerodynamic coefficients differ from its static values if the trailing edge is moved, see Figure 1. The authors analyzed the phase shift between trailing-edge motion and lift coefficient, and the amplitude of the lift coefficient. The results showed a phase shift which increases and an amplitude which decreases with increasing frequency of the trailing-edge motion. Bergami [4] developed an aerodynamic model to account for steady and dynamic effects of a profile with deformable trailing edge of 10% length as a fraction of chord. The model was used within the aeroelastic simulation code HAWC2 to evaluate two different control algorithms. The simulations predicted a load alleviation up to 30%.

The present study focuses on the development of an empirical model which accounts for the transient effects during the trailing-edge motion. This model can then be used within a wind turbine simulation environment to calculate the loads acting on the wind turbine blade. Time-resolved two-dimensional CFD simulations with defined trailing-edge oscillations are carried out for a set of varying parameters. A dependency between the time series of the aerodynamic coefficients and the varied parameters (frequency and amplitude of trailing-edge motion, angle of attack) is found, such that the time series become reproducible as a function of the parameters. Finally, the model is validated by CFD simulations to evaluate if the model is able to reconstruct the results of the fluid simulations and consequently predict the dynamic parts of the aerodynamic coefficients (e.g. $C_{l,\mathrm{Dyn}}$).

2. Airfoil Geometry

The DU08-W-180-6.5 airfoil designed at the TU Delft [10] is used to develop the model (see also Wolff et al. [8]). The deformable trailing edge is represented by a flexible section between $x/c = 0.75$ and $x/c = 0.85$ (c represents the chord length). The rear section between $x/c = 0.85$

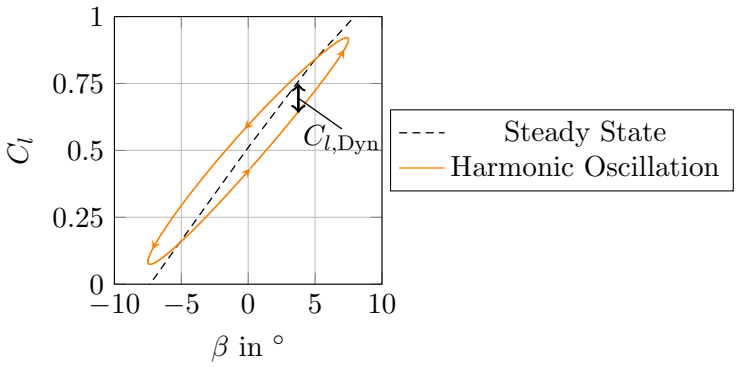

Figure 1. Lift coefficient C_l plotted against the deflection angle β for steady state and at a trailing-edge oscillation with a reduced frequency $k = 0.0875$

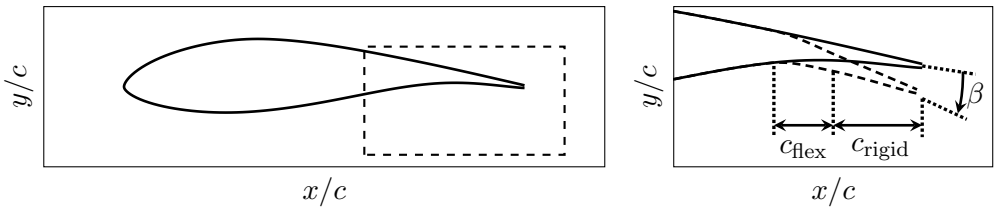

(a) Reference airfoil (b) Trailing edge - Detailed view

Figure 2. Geometry of the DU08-W-180-6.5 airfoil with undeflected trailing edge (——) and with $\beta = 10°$ deflected trailing edge (----), $c_{\text{flex}} = 0.1 \cdot c$, $c_{\text{rigid}} = 0.15 \cdot c$

and $x/c = 1$ is realized as a rigid deflection. A detailed view of the undeflected trailing edge and the $\beta = 10°$ deflected trailing edge is shown in Figure 2b.

3. Numerical Model

3.1. Solver

The aerodynamic design code FLOWer, developed by the German Aerospace Center (DLR) and Airbus Germany [11], is used for the numerical simulations. FLOWer uses structured multi-block meshes and a finite-volume approach to solve the two- and three-dimensional RANS equations. The closure problem of the Reynolds equations is solved by substituting the Reynolds-stress tensor by a two-equation SST k-ω model, see Menter [12]. All boundary layers are assumed to be fully turbulent. The time-resolved simulations are solved by a second-order accurate implicit dual-time stepping scheme. The morphing trailing edge is simulated by a deformable grid approach, which uses linear interpolation to interpolate between given meshes. The time step is set to $\Delta t = 0.00175$ s.

3.2. Mesh

The computational region consists of the two-dimensional airfoil surrounded by a C-H-grid (see Figure 3) with a radius of $50{\cdot}c$ to ensure that there are no reflecting influences from the boundaries. The first cell distance normal to the airfoil surface was defined to be small enough so that the dimensionless wall distance equals $y^+ \approx 1$. The boundary layer region is resolved with 48 cell layers in the direction normal to the airfoil surface, and the whole mesh consists of approximately 85.000 nodes. A grid convergence study has been conducted in accordance with the ASME V & V 20 Committee [13] to determine the discretization error. The results for a conservative calculation order of $p = 1$ show a GCI for the used grid of $GCI_{C_l} = 0.9\%$

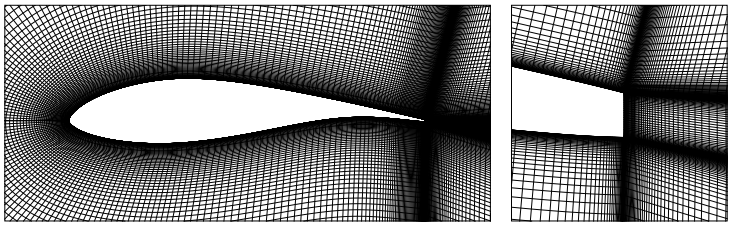

(a) Overview (b) Trailing edge

Figure 3. Computational grid around the airfoil and detailed view on the trailing-edge grid with undeflected trailing edge

concerning the lift coefficient C_l and $GCI_{C_d} = 4.7\%$ concerning the drag coefficient C_d. For a more detailed explanation, see Wolff and Seume [9].

3.3. Boundary Conditions
The boundary of the computational region is set as a farfield boundary and the airfoil surface is defined as a no-slip wall. The Reynolds number is set as $\mathrm{Re} = 7.31 \cdot 10^6$ at the design tip speed and the Mach number is chosen as $\mathrm{Ma} = 0.236$. The angle of attack is varied between $\alpha = 0°$ and $\alpha = 10°$ in steps of $\Delta\alpha = 2°$. 14 different reduced frequencies

$$k = \frac{\omega \cdot c}{2 \cdot U}, \tag{1}$$

(ω represents the angular velocity of the trailing-edge motion and U the flow velocity) are examined for each angle of attack in order to describe the trailing-edge motion. Four different deflection amplitudes $\hat{\beta}$ are chosen between $2.5° \leq \hat{\beta} \leq 10°$. In overall, 336 simulations are performed, each of them taking between 10 and 100 processor hours to calculate. The amount of calculations can be decreased for the model tuning depending on the modeling borders and scope of application.

4. Empirical Model (EM)
The dynamic behavior of a wind turbine blade undergoing changes in the angle of attack has already been modeled in previous work (see e.g. [14] and [15]). The model developed by Hansen et al. [15] has been combined with a model from Gaunaa [16] for the use of a wind turbine blade equipped with a movable trailing edge (see [4]). Most of such models follow complex formulations and/or use high-order derivatives, which can lead to decreased robustness.

Hence, the aim of the model developed in the current work is to use a low-complexity approach using at the most a first derivative of the trailing edge deflection. This aims at a less complicated implementation combined with high robustness. The low-complexity approach can lead to less precise results. Thus, it must be investigated whether the less complex model generates sufficiently accurate results.

4.1. Development
The model accounts for the dynamic parts of the aerodynamic coefficients. The dynamic part $C_{\{l,d,m\},\mathrm{Dyn}}$ is the difference between the transient $C_{\{l,d,m\},\mathrm{Tran}}$ and the static value $C_{\{l,d,m\},\mathrm{Stat}}$ of the aerodynamic coefficient

$$C_{\{l,d,m\},\mathrm{Dyn}} = C_{\{l,d,m\},\mathrm{Tran}} - C_{\{l,d,m\},\mathrm{Stat}} \tag{2}$$

at the same deflection angle β (see Figure 1). Flow simulations of the harmonic trailing-edge oscillation with varying reduced frequency k, deflection angle amplitude $\hat{\beta}$, and angle of attack α are used to simulate the time series of the dynamic parts $C_{\{l,d,m\},\mathrm{Dyn,CFD}}(t)$. The time series are Fourier analyzed

$$C_{\{l,d,m\},\mathrm{Dyn,CFD}}(t) = a_{\{l,d,m\},0} + \sum_{\mathrm{n}=1}^{3} \hat{a}_{\{l,d,m\},\mathrm{n}} \cdot \cos(n \cdot t + \varphi_{\{l,d,m\},\mathrm{n}}) \tag{3}$$

(a, $\hat{a}_n$, and φ represent the Fourier coefficients, t represents the time). The harmonic approach was chosen because all the time series of the dynamic parts show a harmonic behavior (see Figure 4). It is observed that most of the cases have a second harmonic component oscillating with twice the trailing edge's oscillation frequency. This second harmonic component necessitates a

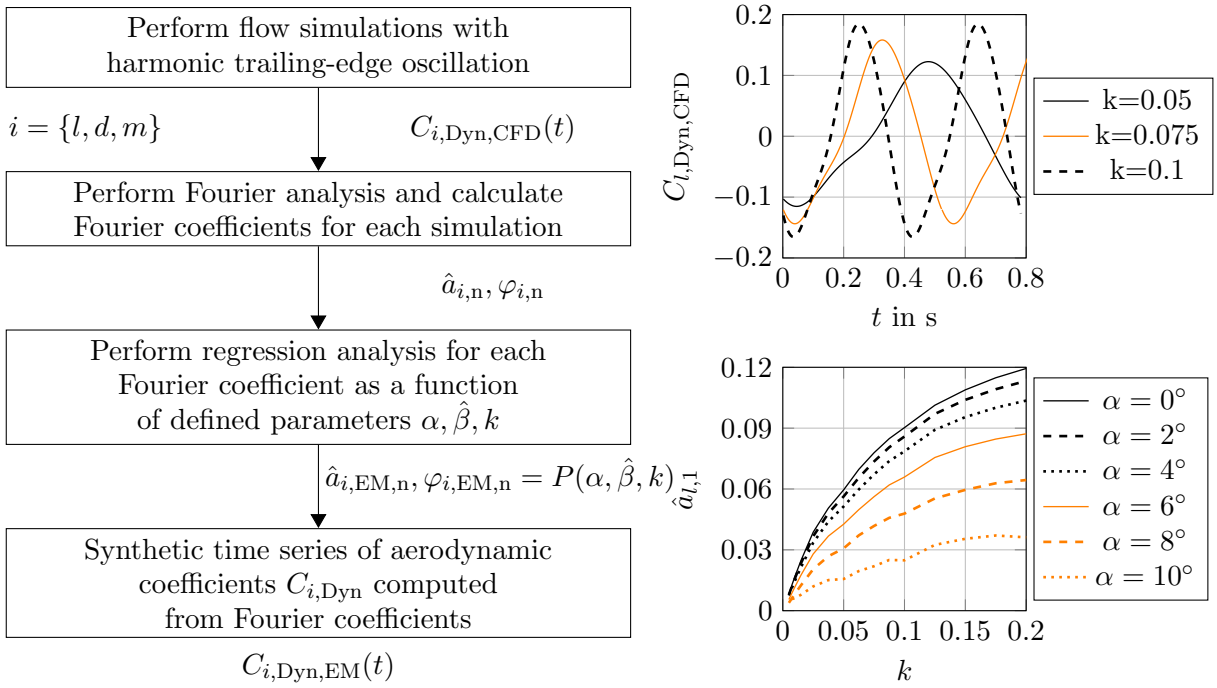

Figure 4. Flow chart of the empirical model's development and examples for the time series of $C_{l,\mathrm{Dyn,CFD}}$ and the first Fourier amplitude $\hat{a}_{l,1}$ as a function of the reduced frequency k

Fourier analysis higher than first degree. Hence, a third degree Fourier analysis is chosen to reach a fitting error less than 0.1%. If lower degree Fourier analyses are chosen, the fitting error will increase to around 20%-30% (first degree) or to around 1%-5% (second degree).

A regression analysis with a third degree polynomial base function

$$P(k, \hat{\beta}, \alpha) = p_0 + p_{\alpha_1}\alpha + p_{\alpha_2}\alpha^2 + p_{\alpha_3}\alpha^3 + p_{\hat{\beta}_1}\hat{\beta} + p_{\hat{\beta}_2}\hat{\beta}^2 + p_{\hat{\beta}_3}\hat{\beta}^3 + p_{k_1}k + p_{k_2}k^2 + p_{k_3}k^3 \quad (4)$$

(P represents the polynomial function and p the polynomial coefficients) is used to reproduce each Fourier coefficient as a function of the defined parameters

$$\hat{a}_{\{l,d,m\},\mathrm{EM,n}},\ \varphi_{\{l,d,m\},\mathrm{EM,n}} = P(k, \hat{\beta}, \alpha). \quad (5)$$

Finally, the time series of the dynamic parts of the aerodynamic coefficients can be calculated out of the reproduced Fourier coefficients

$$C_{\{l,d,m\},\mathrm{Dyn,EM}}(t) = a_{\{l,d,m\},\mathrm{EM},0} + \sum_{\mathrm{n}=1}^{3} \hat{a}_{\{l,d,m\},\mathrm{EM,n}} \cdot \cos(n \cdot t + \varphi_{\{l,d,m\},\mathrm{EM,n}}) \quad (6)$$

An overview of the process is shown in Figure 4.

The non-circulatory forces have a significant influence on the dynamic forces (see Theodorsen [17]). The non-circulatory forces are taken into account by the flow simulations. Consequently, the developed model accounts for these forces as it uses the fourier-analyzed time series of the flow simulations. The dynamic response of the angle of attack was not taken into account because the developed model focuses on moving trailing edges. The developed model could be coupled with existing dynamic stall models implemented in wind turbine simulation environments to account for the dynamic response of the angle of attack.

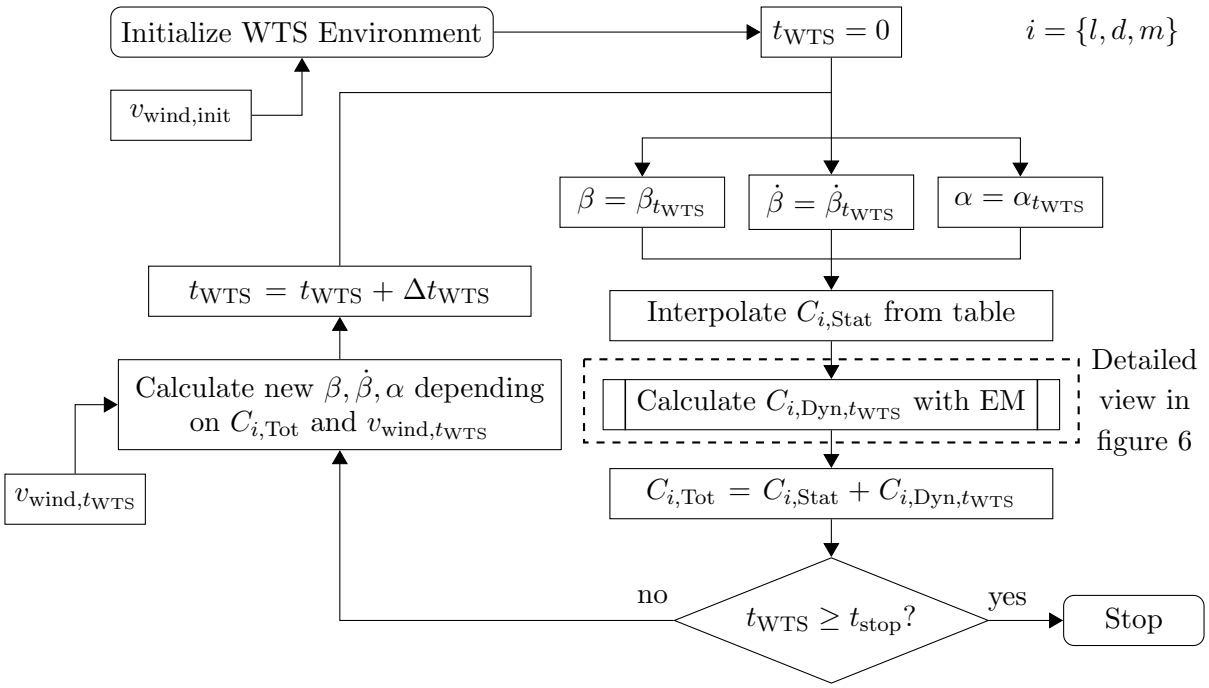

Figure 5. Flow chart of the intended use of the empirical model (EM) within the wind turbine simulation (WTS) environment

4.2. Intended Use

The empirical model is intended to be used within a wind turbine simulation environment (WTS). The WTS simulates the time series of the loads acting on a wind turbine. These loads are calculated depending on the aerodynamic coefficients. Even if most of the common WTS (e.g. HAWC2 and FAST) take dynamic effects during changes in the angle of attack α into account, most of them do not consider the dynamic parts of the aerodynamic coefficients during the motion of the trailing edge. Thus, using the empirical model in a WTS increases the accuracy of the load calculation with moving trailing edges. A flow chart of the empirical model's intended use within the WTS is shown in Figure 5.

The static parts of the aerodynamic coefficients $C_{\{l,d,m\},\mathrm{Stat}}$ are calculated at each of the WTS' time steps as a function of the angle of attack α and the deflection angle β. In general, these values are interpolated from a given table. Thus, the input data for the static coefficients is known.

The dynamic parts of the aerodynamic coefficients $C_{\{l,d,m\},\mathrm{Dyn}}$ depend on the reduced frequency k, the amplitude of the deflection angle $\hat{\beta}$, and the angle of attack α as shown in equation 5. An additional input parameter, the time change of the deflection angle $\dot{\beta}$ given from the trailing-edge controller, is needed to calculate the reduced frequency k. The calculated reduced frequency k in combination with the deflection amplitude $\hat{\beta}$ represent a time series of the deflection angle which is unique for β and $\dot{\beta}$ at the actual WTS' time step.

The empirical model determines the reduced frequency k out of a set of deflection angle time series at which β and $\dot{\beta}$ are present at the same time value t_{EM} using an estimated amplitude

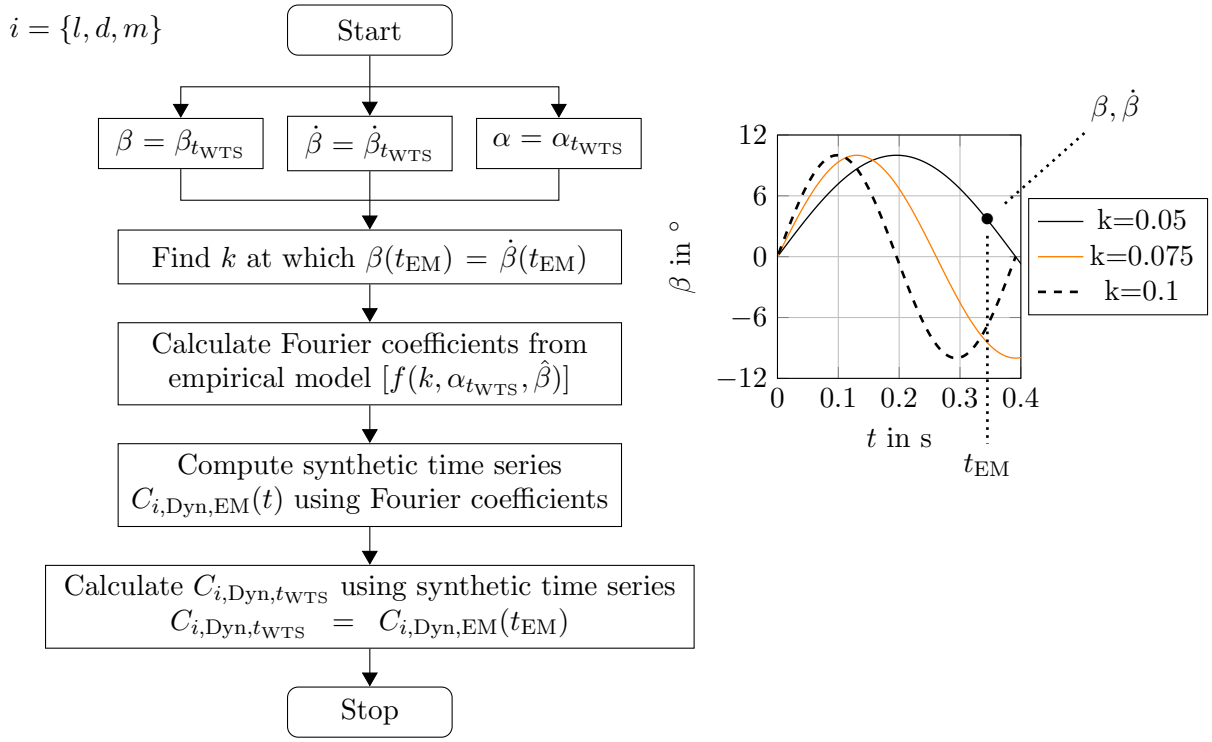

Figure 6. Detailed view on the empirical model (EM) with an example for the identification of the reduced frequency k

of the deflection angle $\hat{\beta}$ (see also Figure 6):

$$\beta(t_{\mathrm{EM}}) = \hat{\beta} \cdot \sin\left(2 \cdot \pi \cdot k \cdot t_{\mathrm{EM}}\right), \tag{7}$$

$$\dot{\beta}(t_{\mathrm{EM}}) = 2 \cdot \pi \cdot k \cdot \hat{\beta} \cdot \cos\left(2 \cdot \pi \cdot k \cdot t_{\mathrm{EM}}\right), \tag{8}$$

$$\rightarrow k = \frac{\dot{\beta}(t_{\mathrm{EM}})}{2 \cdot \pi \cdot \sqrt{\hat{\beta}^2 - \beta(t_{\mathrm{EM}})^2}}, \tag{9}$$

$$\rightarrow t_{\mathrm{EM}} = \frac{\arcsin\left(\beta(t_{\mathrm{EM}})/\hat{\beta}\right) \cdot \sqrt{\hat{\beta}^2 - \beta(t_{\mathrm{EM}})^2}}{\dot{\beta}(t_{\mathrm{EM}})}. \tag{10}$$

A Maximum and minimum value for the amplitude of the deflection angle is set to ensure that the amplitude of the deflection angle does not exceed the borders between which the numerical simulations were performed. Hence, the amplitude of the deflection angle is estimated as follows:

$$\hat{\beta} = \min\left[\max\left(2.5°, AF \cdot |\beta|\right), 10\right]. \tag{11}$$

The amplification factor AF was empirically determined to $AF = 3$. The deflection angle $\hat{\beta}$, the reduced frequency k, and the angle of attack α are used to calculate the Fourier coefficients from the empirical model. These can then be used to calculate a synthetic time series of the aerodynamic coefficients' dynamic parts $C_{\{l,d,m\},\mathrm{Dyn,EM}}(t)$. The dynamic part of the aerodynamic coefficients $C_{\{l,d,m\},\mathrm{Dyn},t_{\mathrm{WTS}}}$ is found at the time t_{EM} at which β and $\dot{\beta}$ are present.

The total aerodynamic coefficients $C_{\{l,d,m\},\mathrm{Tot}}$ (sum of the static and dynamic parts) can be calculated afterwards. These are first used to calculate the loads on the blade with a blade

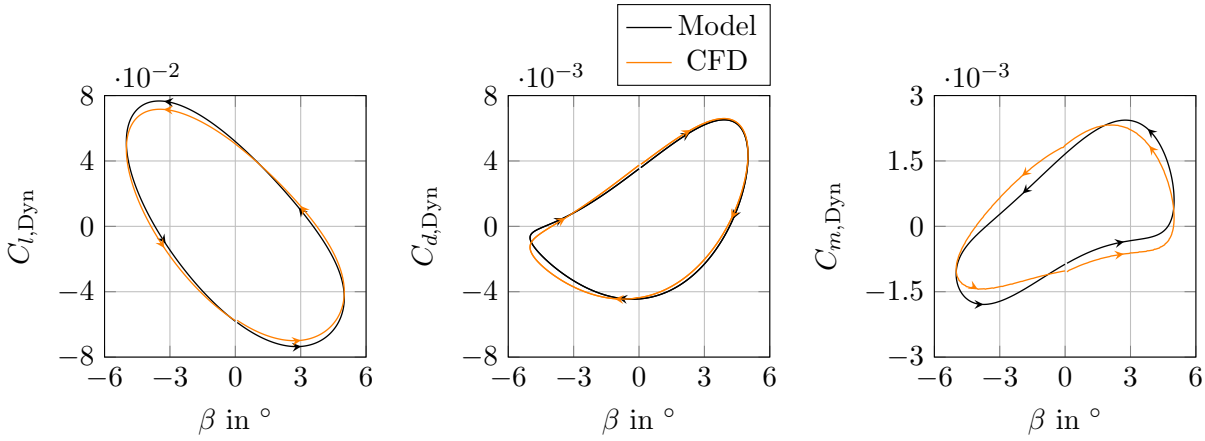

(a) $C_{l,\mathrm{Dyn}}$ (b) $C_{d,\mathrm{Dyn}}$ (c) $C_{m,\mathrm{Dyn}}$

Figure 7. Dynamic parts of the aerodynamic coefficients $C_{l,\mathrm{Dyn}}$, $C_{d,\mathrm{Dyn}}$, and $C_{m,\mathrm{Dyn}}$ plotted against the deflection angle β; $k = 0.0625$, $\alpha = 0°$

element momentum method. Afterwards, the total aerodynamic coefficients are used by the wind-turbine controller to define new values for α, β, and $\dot{\beta}$, depending on the new wind speed $v_{\mathrm{wind},t_{\mathrm{WTS}}}$ at the next time step t_{WTS}. The loop continues until the defined stopping criteria of the WTS is reached.

4.3. Model Fit and Validation

The empirical model is implemented in the numerical computing environment *MATLAB* to validate that it's results are reasonable. First, defined oscillations of the trailing edge with varying parameters α, $\hat{\beta}$, and k are simulated once with the empirical model and once with CFD. The results of both simulation methods are compared to each other to make sure that the Fourier and regression analysis give reasonable results. The hysteresis loops of the aerodynamic coefficients' dynamic parts are shown in Figure 7 as a function of the transient deflection angle β. The negligible deviations between empirical model and CFD prove that the CFD results can be reconstructed with the empirical model in the current case. This is the same for most of the other configurations. However, there are some cases, especially near stall, which show discrepancies between the modeled data and the CFD results. These discrepancies can be explained by the low-complexity approach of the model. Non-linear effects are not taken into account and the model does not differentiate between attached and near-stall flow. This limits the bandwidth of angles of attack, which can be accurately modeled.

Random series of the deflection angle at six different angles of attack $0° \leq \alpha \leq 10°$ are used for the model validation. These series are calculated with CFD and with the developed model. Such a validation with random time series has, to the authors' knowledge, not been carried out for any of the previously developed models because these models were validated with harmonic time series. The dynamic parts of the lift coefficient are shown in Figure 8 for both calculations at three of the six different angles of attack α. The modeled results fit the CFD results at low angles of attack ($\alpha < 4°$, see Figure 8b). The fit gets worse towards higher angles of attack up to $\alpha = 10°$, at which both results no longer fit each other (see Figure 8d).

The opposite case appears at the modeled drag coefficient, shown in Figure 9. The results of the model and the CFD do not fit each other at low angles of attack $\alpha < 4°$, see Figure 9b. At higher angles of attack, e.g. $\alpha = 4°$ (Figure 9c) and especially $\alpha = 10°$ (Figure 9d), the modeled results fit the CFD results.

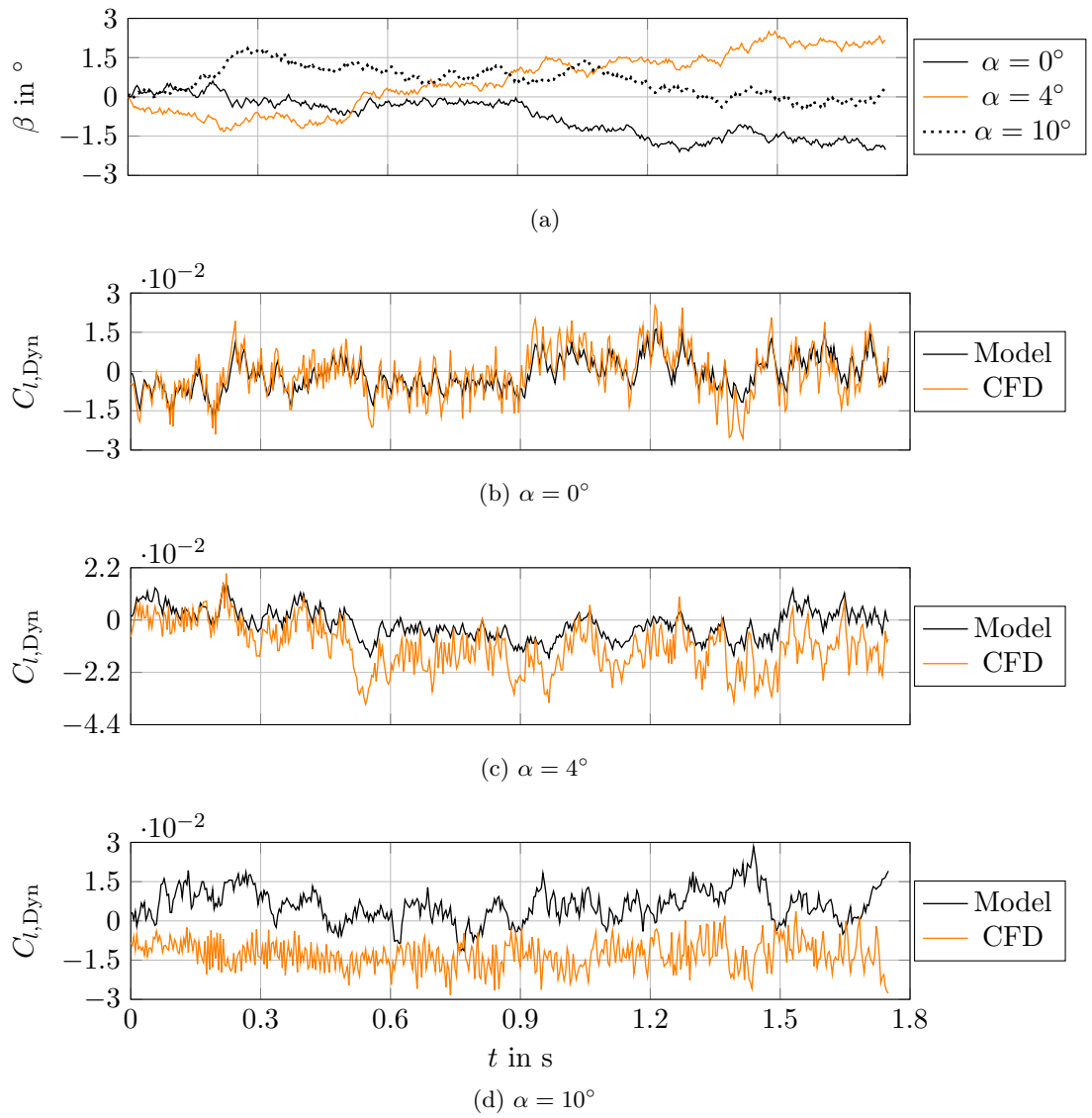

Figure 8. Dynamic parts of the lift coefficient $C_{l,\mathrm{Dyn}}$ plotted against the time t for the modeled and CFD-simulated data at constant angles of attack $\alpha = 0°, \alpha = 4°$, and $\alpha = 10°$

The reason for the conversely fit results of the dynamic lift and drag coefficient is the fit of the regression analysis. The fit of the regression analysis increases towards lower angles of attack for the lift coefficient and towards higher angles of attack for the drag coefficient. Thus, the modeling quality of the fourier coefficients and consequently of the dynamic coefficients increases towards lower angles of attack for the lift coefficient and towards higher angles of attack for the drag coefficient.

5. Conclusions

The empirical model developed in the present work aims to account for transient effects during the motion of a morphing trailing edge. The model is based on Fourier-analyzed time series of the aerodynamic coefficients' dynamic parts, generated by fluid simulations. Numerous simulations with varying angle of attack α, amplitude of the trailing-edge deflection $\hat{\beta}$, and reduced frequency k have been performed to build a solid ground for the model.

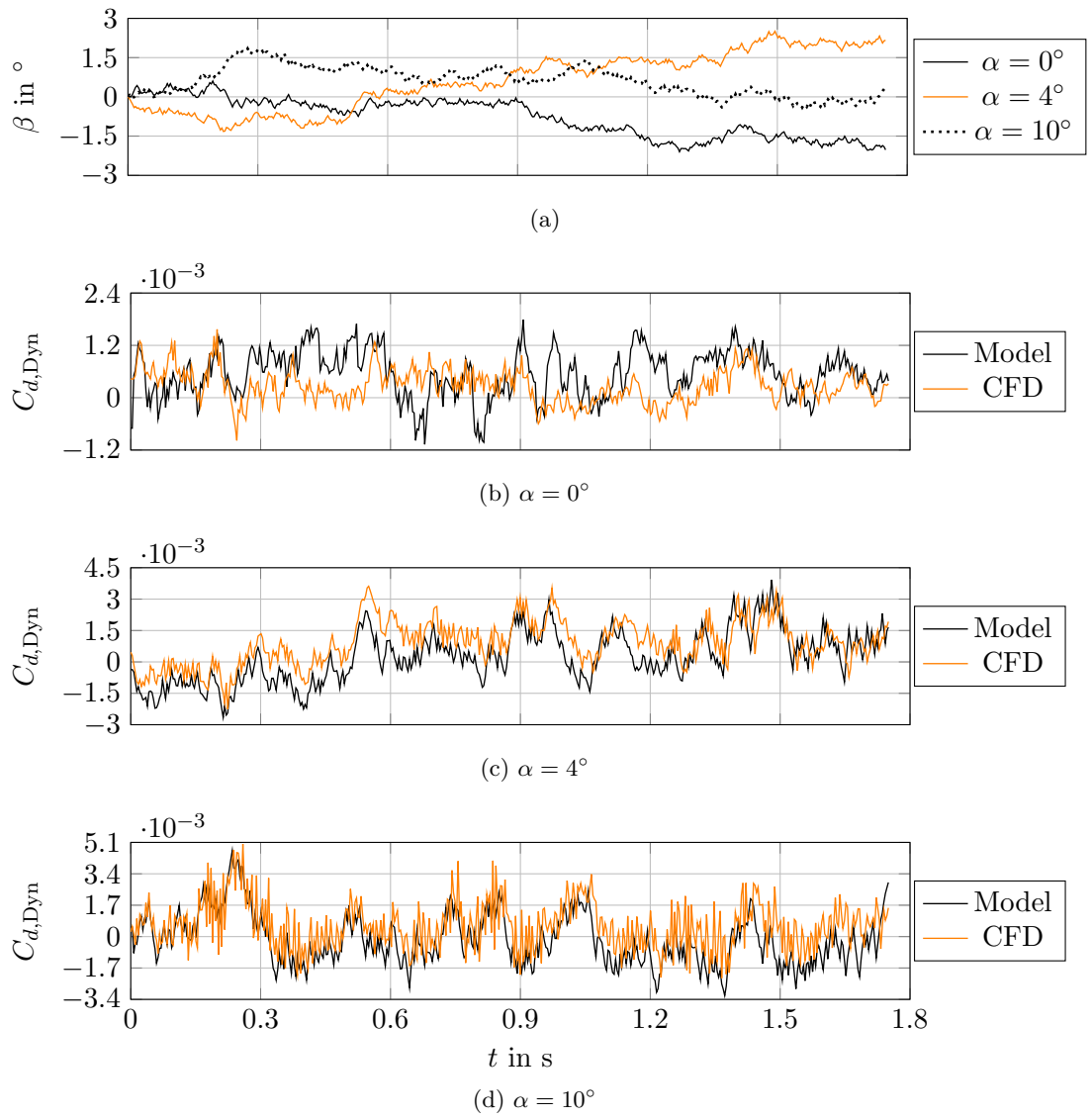

Figure 9. Dynamic parts of the drag coefficient $C_{d,\mathrm{Dyn}}$ plotted against the time t for the modeled and CFD-simulated data at constant angles of attack $\alpha = 0°, \alpha = 4°$, and $\alpha = 10°$

The present results generated with the model show that the empirical model is able to reconstruct CFD results in case of harmonic trailing-edge oscillations. The test cases used to evaluate the model fit show merely negligible deviations between modeled and CFD results. Slightly higher deviations are observed at some cases, especially near stall, due to the low-complexity approach. Hence, the dynamic parts of the aerodynamic coefficients $C_{l,\mathrm{Dyn}}$, $C_{d,\mathrm{Dyn}}$, and $C_{m,\mathrm{Dyn}}$ can be modeled by a Fourier analysis, at least for attached flows.

Even in case of a random trailing-edge motion, the modeled results fit the CFD results over a limited range of angles of attack. The modeled lift coefficient is in overall in consistence with the CFD results at low angles of attack ($\alpha < 4°$). The discrepancies between the two simulation methods increase towards higher angles of attack. Conversely, the drag coefficients show discrepancies between model and CFD at low angles of attack and a good fit towards high angles of attack. This leads to the conclusion that the regression analysis used for the reproduction of the Fourier coefficients is able to fit the parameter curves in defined bands of

the angle of attack, but does not generate reasonable results for other values of the angle of attack.

Consequently, the regression analysis will be differentiated into two parts in future studies, one at attached flow and one near stall. Possible discontinuity problems will be avoided by using a weighting function for the transition from attached to near-stall flow. Additionally, the validation has to be expanded: Different airfoils have to be taken into account as well as the model fit outside the parameter's tuning range. If this leads to satisfying results, the model will be implemented in a wind turbine simulation environment to calculate the loads of a wind turbine.

Acknowledgments

The present work is funded within the framework of the joint project Smart Blades (0325601A/B/C/D) by the German Federal Ministry for Economic Affairs and Energy (BMWi) under decision of the German Federal Parliament. The authors appreciate the German Aerospace Center (DLR) for providing FLOWer. The authors thank the Leibniz Universitaet Hannover IT Services (LUIS) for the computational resources provided.

References

[1] Kaldellis J K and Zafirakis D 2011 *The wind energy (r)evolution: A short review of a long history* pp 1887–1901 Renewable Energy **36**
[2] Kelley N, Hand M, Larwood S and McKenna E 2002 *The NREL large-scale turbine inflow and response experiment - Preliminary results* ASME Wind Energy Symp. (Reno, Nevada) WIND2002-64 pp. 412-26
[3] Barlas T K and van Kuik G A M 2007 *State of the art and prospectives of smart rotor control for wind turbines* J. Phys.: Conf. Ser. **75** 012080
[4] Bergami L 2013 *Adaptive Trailing Edge Flaps for Active Load Alleviation in a Smart Rotor Configuration* DTU Wind Energy PhD-0020(EN)
[5] Pechlivanoglou G K, Wagner J, Nayeri C N and Paschereit C O 2010 *Active aerodynamic control of wind turbine blades with high deflection flexible flaps* 48th AIAA Aerospace Sciences Meeting (Orlando, Florida) AIAA 2010-644
[6] Bak C, Gaunaa M, Andersen P B, Buhl T, Hansen P, Clemmensen K and Moeller R 2007 *Wind tunnel test on wind turbine airfoil with adaptive trailing edge geometry* 45th AIAA Aerospace Sciences Meeting and Exhibit (Reno, Nevada) AIAA 2007-1016
[7] Troldborg N 2005 *Computational study of the Riso-B1-18 airfoil with a hinged flap providing variable trailing edge geometry* pp 89–113 Wind Engineering **29** (2)
[8] Wolff T, Ernst B and Seume J R 2014 *Aerodynamic behavior of an airfoil with morphing trailing edge for wind turbine applications* J. Phys.: Conf. Ser. **524** 012018
[9] Wolff T and Seume J R 2015 *Airfoil with morphing trailing edge for load reduction in wind turbines* 33rd Wind Energy Symposium (Kissimmee, Florida) AIAA 2015-1662
[10] Timmer N and van Rooij R 2009 *Summary of the delft university wind turbine dedicated airfoils* Tech. rep. TU Delft
[11] Kroll N and Fassbender J K 2002 *MEGAFLOW - Numerical flow simulation for aircraft design* (Berlin: Springer)
[12] Menter F 1994 *Two-Equation Eddy-Viscosity Turbulence Models for Engineering Applications* pp 1598–1605 AIAA Journal **32**
[13] ASME V & V 20 Committee 2009 *Standard for verification and validation in computational fluid dynamics and heat transfer* (New York, USA: The American Society of Mechanical Engineers)
[14] Rasmussen F, Petersen J T and Madsen H A 1999 *Dynamic Stall and Aerodynamic Damping* pp 150–155 Journal of Solar Energy Engineering **121**
[15] Hansen M H, Gaunaa M and Madsen H A 2004 *A Beddoes-Leishman type dynamic stall model in state-space and indicial formulations* Tech. rep. r-1354(EN), Risoe National Laboratory (Roskilde, DK)
[16] Gaunaa M 2010 *Unsteady two-dimensional potential-flow model for thin variable geometry airfoils* pp 167–192 Wind Energy **13**
[17] Theodorsen T 1935 *General Theory of Aerodynamic Instability and the Mechanism of Flutter* Tech. rep. **496**, National Advisory Committee for Aeronautics